

Mechanical Properties and Wear Behavior of AA5182/WC Nanocomposite Fabricated by Friction Stir Welding at Different Tool Traverse Speeds

Moslem Paidar, Ali Asgari, Olatunji Oladimeji Ojo, and Abbas Saberi

(Submitted August 5, 2017; in revised form February 28, 2018; published online March 20, 2018)

Grain growth inhibition at the heat-affected zone, improved weld strength and superior tribological properties of welds are desirable attributes of modern manufacturing. With the focused on these attributes, tungsten carbide (WC) nanoparticles were employed as reinforcements for the friction stir welding of 5-mm-thick AA5182 aluminum alloy by varying tool traverse speeds. The microstructure, microhardness, ultimate tensile strength, fracture and wear behavior of the resultant WC-reinforced welds were investigated, while unreinforced AA5182 welds were employed as controls for the study. The result shows that the addition of WC nanoparticles causes substantial grain refinement within the weld nugget. A decrease in traverse speed caused additional particle fragmentation, improved hardness value and enhanced weld strength in the reinforced welds. Improved wear rate and friction coefficient of welds were attained at a reduced traverse speed of 100 mm/min in the WC-reinforced welds. This improvement is attributed to the effects of reduced grain size/grain fragmentation and homogeneous dispersion of WC nanoparticles within the WC-reinforced weld nugget.

Keywords AA5182/WC nanocomposite, friction stir welding, mechanical properties, microstructural characteristics, WC nanoparticles

1. Introduction

The needs for improved surface properties and weld nugget quality in contemporary manufacturing have engendered studies into the reinforcement of aluminum alloys with carbides, nitrides, borides, and oxides in the form of particles, whiskers, and fibers (Ref 1). Homogeneous distribution of these reinforcements in aluminum matrices is critical to attaining the desired surface and weld properties. This phenomenon can be achieved via the use friction stir welding (FSW) or processing due to the welding tool's rotational effect and non-fusion welding temperature (less than 80% of the melting temperature of the Al) of FSW. FSW process inhibits decomposition of reinforcements and prevents uncharacteristic interaction between reinforcement and Al matrices. The dispersed reinforcements in the weld nugget inhibit grain growth and even when the weld is subjected to post-weld treatment, abnormal grain growth is always prevented (Ref 2).

Literature has shown that abrasion resistance or wear rate of reinforced aluminum alloys have been improved via friction stir welding/processing. Yuvaraj et al. (Ref 3) worked on FSW of AA5083 alloy with reinforced layers of micro and nano-sized

boron carbide (B_4C) particles. It was revealed that the number of passes and particle size greatly influenced the surface characteristics of the resultant composite. Sudhakar et al. (Ref 4) improved wear and ballistic resistance of AA7075 alloy when boron carbide was used as the reinforcing particles, while molybdenum disulfate was utilized as a solid lubricant. Palanivel et al. (Ref 5) observed that the morphology of TiB_2 was altered, while that of BN was unaltered after friction stir processing of AA6082/ TiB_2 composite. The BN nanoparticles were affirmed to improve the wear resistance of AA6082/ TiB_2 composite by forming a tribo film and by acting as lubricants.

The works of Sahraeinejad et al. (Ref 6) showed that B_4C reinforced AA5059 alloy produced the highest tensile strength compared to that of Al_2O_3 and SiC, but drastically impaired ductility was attained in the B_4C reinforced weld. A few researchers have worked on the improvement of ductility of aluminum alloys via the replacement of carbides with hard metallic nanoparticles. Selvakumar et al. (Ref 7) utilized hard metallic particles of molybdenum as reinforcement for AA6082 alloy by using friction stir processing in order to improve the ductility of the resultant aluminum matrix composite. It was shown that Mo particles improved the tensile strength and ductility of the fabricated composite. The refined grains were attributed to dynamic recrystallization coupled with pinning effect. Similarly, the use of hard metallic particles (stainless steel particles) as reinforcements for AA6082 alloy improved the tensile strength of the composite without sacrificing its ductility (Ref 8).

In addition to the use of boron carbide (B_4C), boron nitride (BN), and hard metallic nanoparticles (such as molybdenum and stainless steel) as reinforcements, there are other nanopowders/particles that have been employed in improving the mechanical properties of FSW'ed welds. Bodaghi et al. (Ref 9) investigated the effects of SiC nanoparticles on friction stir welding of AA5052 alloy. SiC nanoparticles acted as nucleation sites and also pinned the grain boundaries (impeded

Moslem Paidar and Ali Asgari, Department of Materials Engineering, Islamic Azad University, South Tehran Branch, Tehran, Iran; Olatunji Oladimeji Ojo, Department of Mechanical Engineering Science, The Federal University of Technology Akure, Akure, Nigeria; and Abbas Saberi, Advanced Materials Research Center, Materials Engineering Department, Najafabad Branch, Islamic Azad University, Najafabad, Iran. Contact e-mail: m.paidar@srbiau.ac.ir.

dislocation movement). Thus, reduced grain size via Zener effect was acclaimed to influence hardness increase in the reinforced weld nugget, while powder agglomeration in the stir zone diminished the ultimate tensile strength of the welds. Khorrani et al. (Ref 10) examined the thermal stability of friction stir welded AA1050 alloy with SiC nanoparticles. It was revealed that heat treatment up to 400 °C had no significant influence on the grain growth of the stir zone when the suitable distribution of nanoparticles was established. Improved wear resistance and low friction coefficient of the welds were attributed to the presence of dispersed TiO₂ reinforcement in AA5083 alloy (Ref 2).

A perusal of literature shows that the use of tungsten carbide (WC) nanoparticles as reinforcements for friction stir welding of aluminum alloys is yet to be reported. WC can be an excellent reinforcement alternative considering its characteristics such superior strength/rigidity, low thermal expansion coefficient, wear resistance, and high hardness. In addition, the effect of numbers of passes on welds has been elaborately provided in the literature, but there is still a paucity of information on the influence of traverse speed on reinforced aluminum alloys. As a result, this paper examines the effect of WC nanoparticles/reinforcement on friction stir welds of AA5182 alloy. The corresponding effect of traverse speed on the reinforced weld nugget is examined via microstructural, tribological and mechanical characterizations.

2. Experimental Procedure

In this study, 5-mm-thick AA5182 aluminum alloy plate was employed as the base material. Its tensile strength, yield strength and elongation are 268 MPa, 128 MPa and 19%, respectively. The major chemical compositions of the alloy include 4.2 wt.%Mg, 0.41 wt.%Mn, 0.15 wt.%Si, 0.01 wt.%Ti, and 0.13 wt.%Fe. The reinforcement utilized was tungsten carbide (WC) nanoparticles with an average size of 55 nm. The nanoparticles were viewed in transmission electron microscope (TEM), and the resultant micrograph of the WC nanoparticles is shown in Fig. 1. In order to ensure the containment of WC nanoparticles within the weld line during friction stir welding, a groove with a depth and a width of 0.5 and 1 mm, respectively, was machined on each of the plates' edges to form a furrow when the abutting plates' edges are arranged for FSW process (see Fig. 2a). Thus, prior to the friction stir welding process, rigid clamping of the workpiece was carried out and the milled furrow on the abutting line of the workpiece arrangement was filled with WC nanoparticles.

A cylindrical threaded pin tool made from H13 steel having shoulder diameter, pin height, and pin width diameter of 20, 4.7 and 6 mm, respectively, was fabricated for the FSW process. Figure 2(c) shows the pictorial representation of the welding tool. However, the work is focused on the assessment of the role of traverse speed on welds. As a result, tool rotational speed of 500 rpm was used, while traverse speeds of 100, 200, 300 and 400 mm/min were employed for the entire experiment. Equally, the cross sections of the resultant welds were cut, mounted in epoxy resin, ground and polished until reflective and smooth surfaces were attained. Subsequently, the etching of the prepared samples was carried out in a solution of 2 mL of HF, 3 mL of HCl, 5 mL of HNO₃, and 190 mL of H₂O. Afterward, the samples were viewed under an optical micro-

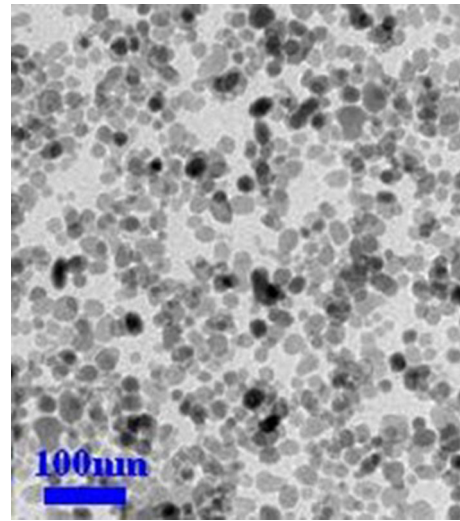


Fig. 1 TEM image of WC nanoparticles

scope (OM) and also in a scanning electron microscope (SEM) in order to analyze the weld's microstructures. Vickers microhardness of welds was determined by applying 200 g load for a dwell time of 15 s. The ultimate tensile strengths of the welds were determined according to ASTM E8M-04 standards (see Fig. 2b) by using an INSTRON 5500R testing machine at a constant displacement rate of 2 mm/min. The fracture surfaces of the resultant failed welds were examined. According to ASTM G99 standards, wear test was performed on the weld samples by using the pin on disk method and 52100 Steel with a hardness of 60 HRC as the counterface material. The employed wear parameters include an applied load, rotating speed and sliding velocity of 40 N, 26.04 rpm and 0.35 mm/s respectively.

3. Results and Discussion

3.1 Surface Appearance

Figure 3 shows the surface appearances of some selected weld specimens obtained at traverse speeds of 400 and 100 mm/min, respectively. It is observed that a change in the tool traverse speed has a considerable effect on the surface appearance of the FSW welds. The results show that weld surface with smoother, un-serrated flow traces and reduced flash is formed at reduced traverse speed. This is attributed to the induced heat input during the welding process. More thermal energy is retained within the stirred zone at reduced traverse speed, and this facilitates better plasticization and material flow (Ref 11). Conversely, it can be seen that semicircular traces were formed on the weld produced at higher traverse speed (Fig. 3a). These occurrences have been referred to as onion rings in the literature. This is in agreement with the works of Mohammadi-pour et al. (Ref 12) as coarser weld surfaces are obtained at high welding speed as compared to low welding speed. It was suggested that the exposure period of the stir zone to tool traverse effect significantly influenced material flow/behavior and the resultant surface appearance of the weld. The formation of flash around the neighboring region

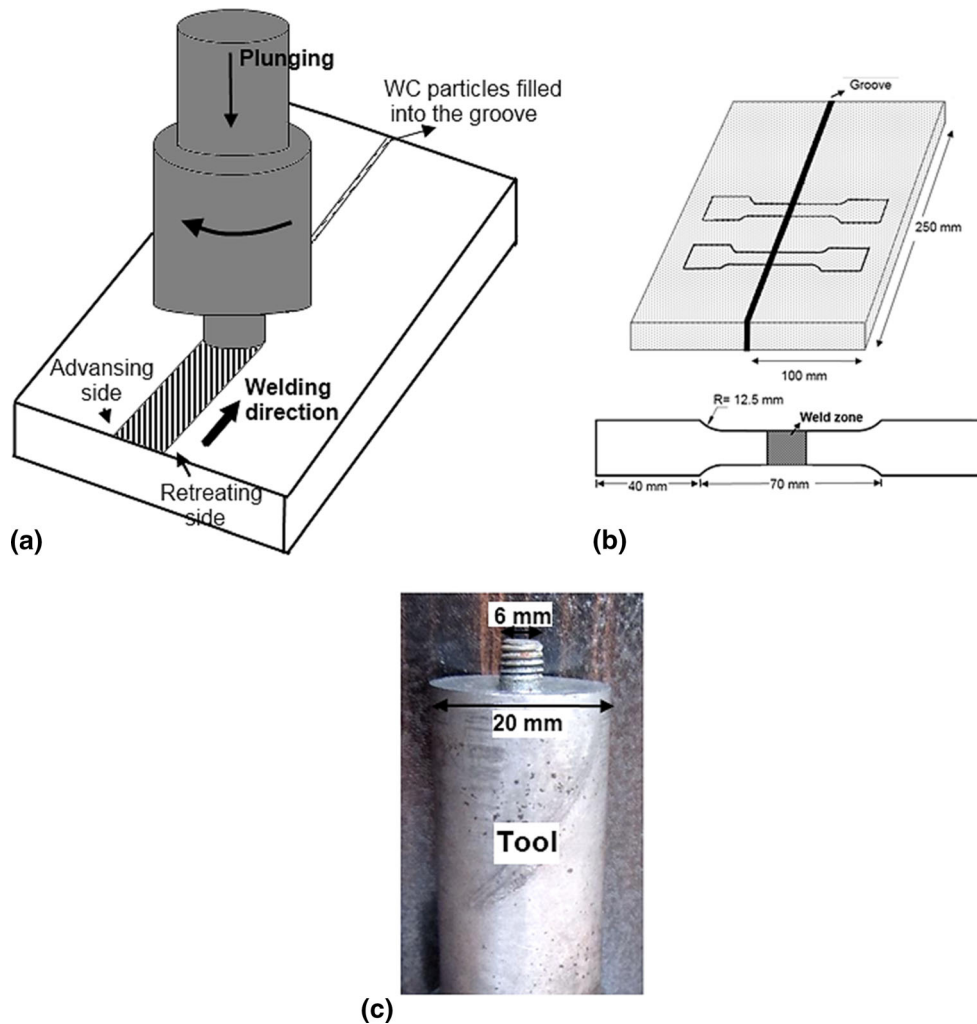


Fig. 2 Illustrations of FSW welding (a) joint configuration, (b) tensile samples, (c) cylindrical threaded pin tool

of the weld nugget is enhanced at increased traverse speed due to high tool-material transport effect.

3.2 Microstructural Features

Figure 4 illustrates the optical micrographs of different regions of the reinforced weld nugget of AA5182 alloy. The cross section of the joints consists of three different regions which are the heat-affected zone (HAZ), thermo-mechanically affected zone (TMAZ), and the stir zone (SZ) as indicated in Fig. 4(b), (c), and (d), respectively. It is evident from the figure that the grains in SZ are very fine and equiaxed. The formation of fine equiaxed recrystallized grains in the SZ can be attributed to dynamic recrystallization (Ref 12-16). According to Fig. 4(c), the microstructure of TMAZ has elongated grains due to the shearing effect induced by the rotational and traversal actions of the tool during the FSW process (Ref 16). It is adjudged that this phenomenon resulted from the presence of severe plastic deformation in the TMAZ. In addition, Fig. 4(b) suggests that the microstructure of the HAZ is similar to that of the BM. A comparison of Fig. 4(b) with that of the BM shows that the microstructure of HAZ is only affected by the thermal energy during FSW process.

Figure 5 reveals the microstructures of the reinforced stir zones obtained at different traverse speeds and at a constant

tool rotational speed of 500 rpm. Disparity in the sizes of grains is observed in Fig. 5, while Fig. 6 affirms that a direct relationship exists between grain size and traverse speed. Average grain sizes of 2.1 and 7.6 μm were obtained in the reinforced welds at traverse speeds of 100 and 400 mm/min, respectively, whereas that of the unreinforced welds had 20 and 35 μm , respectively. This suggests that the addition of WC nanoparticles to the Al alloy prevents grain growth in the resultant weld nugget. This grain refinement occurrence may likely be due to the boundary pinning effect caused by the fragmented WC nanoparticles in the structure of the reinforced welds.

Figure 7 shows the SEM micrographs of welds obtained with and without WC nanoparticles at a constant traverse speed of 300 mm/min. Large grain boundaries with no evidence of reinforced particles are revealed in the unreinforced weld shown in Fig. 7(a). The reinforced weld (Fig. 7b) shows fairly dispersed reinforcements as white particles and smaller grain sizes or boundaries are consequences of the presence of these reinforcements. The WC nanoparticles within the recrystallized aluminum matrix act as restraining particles that impede the movement of grain boundaries/dislocation in the SZ. Paidar et al. (Ref 11) and Bodaghi et al. (Ref 9) reported that the reinforced particles act as barriers against grain boundary

motion and this consequently prevents grain growth due to the restrained grain boundary (Ref 11). The counteraction existing between grain boundary movement and reinforcement particles ensures Zener pinning effect within the SZ to inhibit grain growth. Moses et al. (Ref 17) reported that factors such as better or homogeneous dispersion of reinforcement particles

and increase in the number of grain nucleation sites during solidification could be the cause of this grain refinement or reduced grain sizes, whereas Heidarzadeh et al. (Ref 18) discovered that the nanoparticles restrict the growth of grains by Zener pinning impact.

Figure 8 shows the effect of traverse speed on the distribution of WC nanoparticles in the welds' SZ, while a higher magnification image showing the presence of WC nanoparticles in the aluminum matrix is shown in Fig. 9. The distribution/dispersion and refinement of WC nanoparticles in the SZ of welds decreased with an increase in traverse speed as revealed in Fig. 8. Fragmentation of particles in the SZ of welds is more pronounced as the traverse speed is decreased and this has a direct impact on the resultant grains in the stirred region (see Fig. 5 and 6). Figure 8(d) shows finely fragmented particles at a traverse speed of 100 mm/min as compared to that of 400 mm/min (Fig. 8a). Eftekharinia et al. (Ref 19) reported that wear rate is a function of reinforced particles' distribution in welds. The effect of WC nanoparticles' dispersion on wear rate is thus examined in section 3.3.

3.3 Mechanical Properties

3.3.1 Microhardness. Figure 10 illustrates the variation of Vickers microhardness value as a function of tool traverse speed. The hardness values indicate a somewhat erratic relationship with the traverse speed. The maximum and the least hardness values are obtained at the highest and the least traverse speeds, respectively. Hardness values of 96 and 83 HV were obtained at traverse speeds of 400 and 100 mm/min, respectively.

Vickers microhardness profile of reinforced welds is compared with that of the unreinforced weld in Fig. 11. Welds obtained at the same welding conditions of rotational and traverse speeds of 500 rpm and 300 mm/min were employed

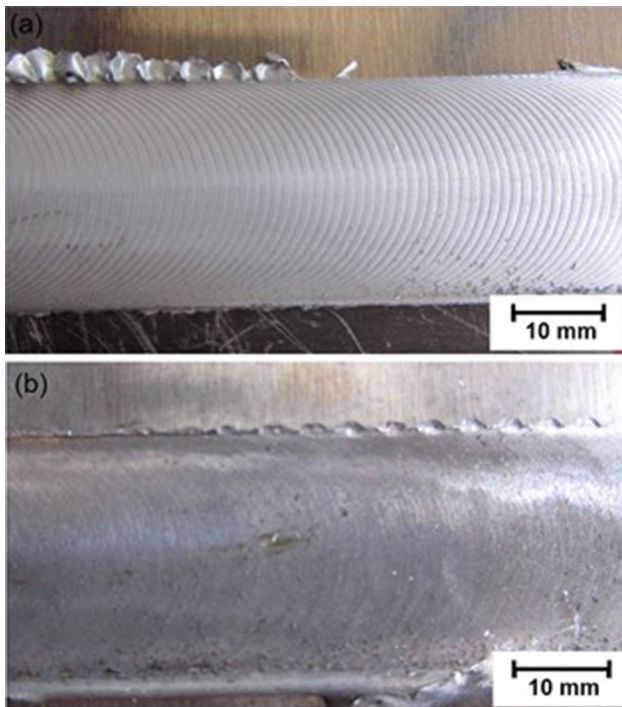


Fig. 3 Surface appearance of joints welded as a function of tool traverse speed, (a) 400 mm/min and (b) 100 mm/min

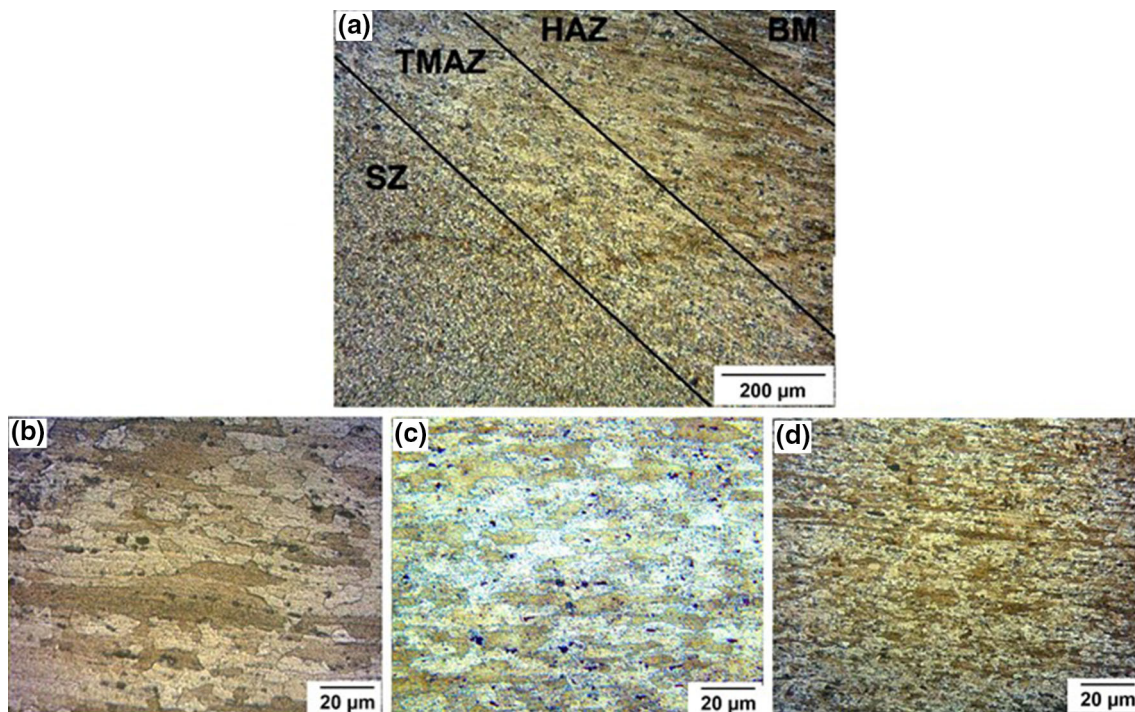


Fig. 4 Microstructures in various zones of FSW AA5182 joints: (a) weld zones, (b) HAZ, (c) TMAZ and (d) SZ

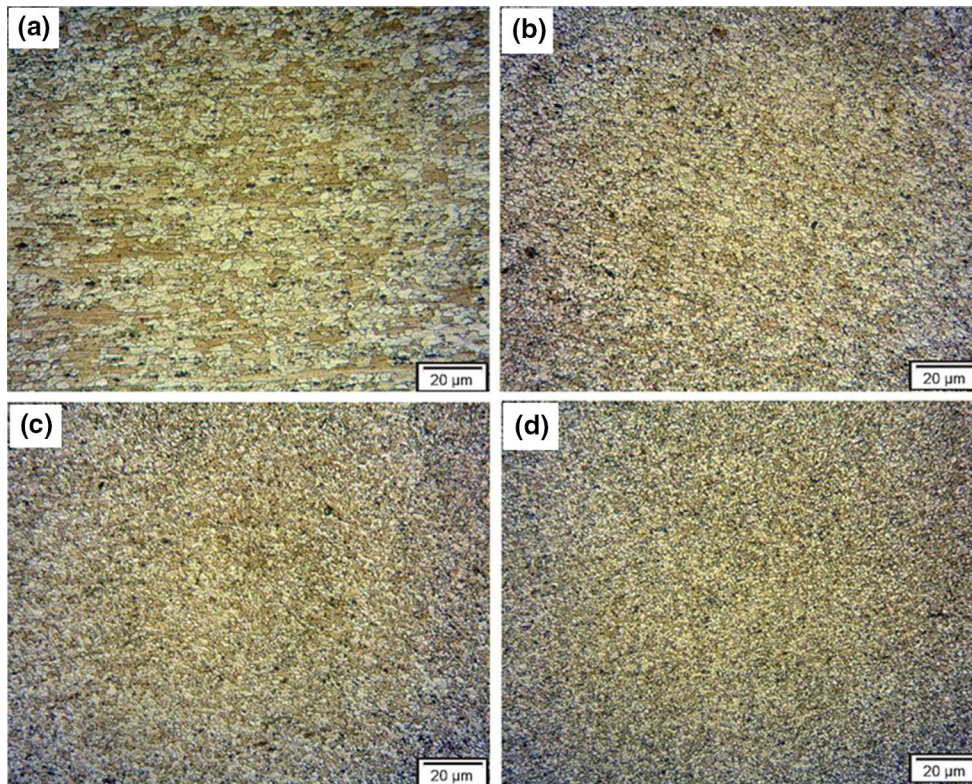


Fig. 5 Microstructure of welds obtained using different traverse speeds, (a) 400, (b) 300, (c) 200 and (d) 100 mm/min

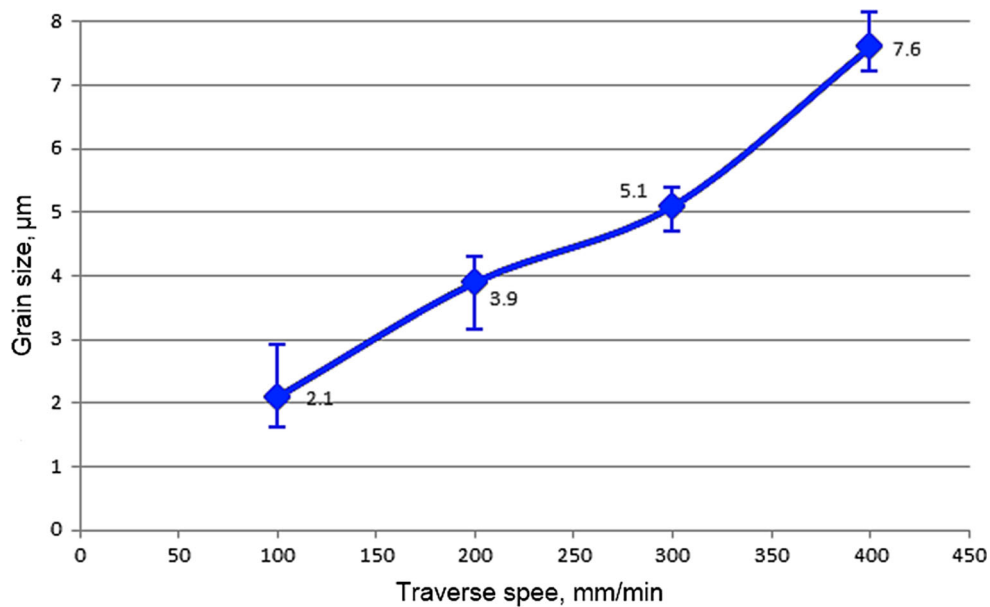


Fig. 6 Relationship between average grain size and traverse speed

for this comparison. It is observed that the addition of WC nanoparticles to the FSW'ed AA5182 alloy significantly improves the weld hardness. This occurrence can be attributed to the inhibition of grain growth due to the presence of WC nanoparticles in the weld nugget of AA5182 alloy (see section 3.2). Hall-Petch relationship is obeyed as welds (reinforced welds) with reduced grain sizes exhibit better microhardness value than welds without reinforcements. A plot

of yield stress against the inverse square root of grain diameter shows a correlation coefficient (R^2) of 0.88, strengthening coefficient (k) of 0.52 MPa mm^{1/2} and 137.46 MPa as lattice friction stress/stress required for dislocation movement. This confirms that grain size reduction increases both the number of grain boundary and hindrance per unit length for the dislocation. The reduced grain size would enforce less dislocation pile up and driving force (at the grain boundary) during the tensile

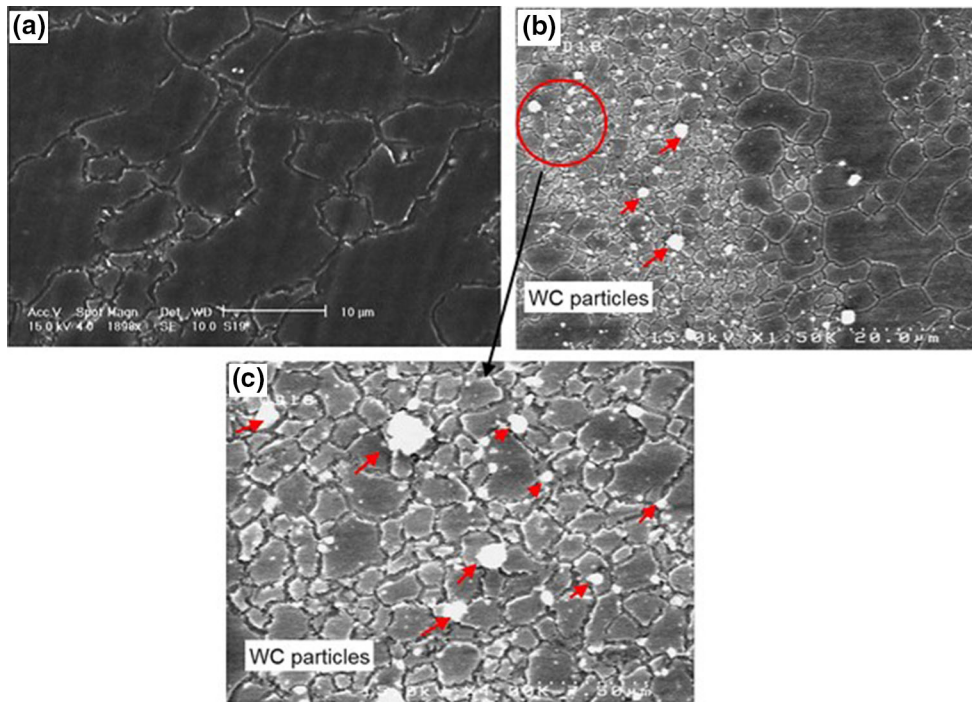


Fig. 7 Microstructure of welds obtained, (a) without WC nanoparticles, (b) with WC nanoparticles and (c) high-magnification SEM images of (b)

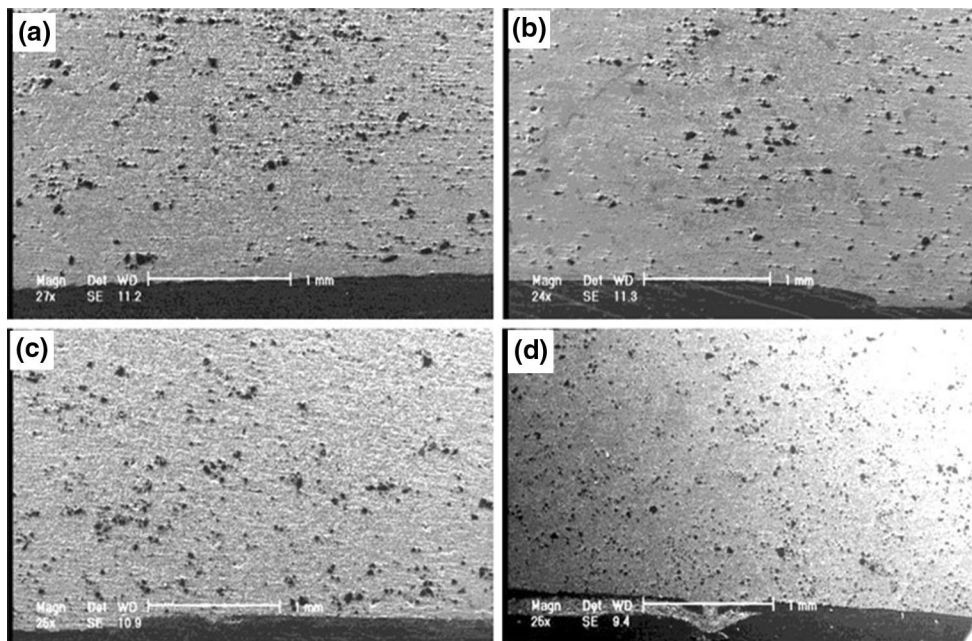


Fig. 8 SEM images of distribution of WC nanoparticles at different traverse speeds, (a) 400, (b) 300, (c) 200 and (d) 100 mm/min

loading condition, and thus, larger applied load/stress would be required to push the dislocation to the next grain. Consequently, improved hardness and strength (See section 3.3.2 and Fig. 6) are attained in the reinforced weld samples with reduced grain sizes.

The effect of traverse speed on Vickers microhardness profile of welds with and without WC nanoparticles is shown in Fig. 12. The hardness values of weld samples with nanoparticles are much higher than that of welds without reinforce-

ments. Maximum hardness value is attained at 100 mm/min in the reinforced welds, and a further increase in the tool traverse speeds from 200 to 400 mm/min produces a somewhat negligible effect on the welds' hardness profile. On the other hand, Fig. 12 shows that increase in the traverse speed directly improves the hardness values of the unreinforced weld nugget of AA5182 alloy. This occurrence is attributed to the propensity of generating lower heat input as the traverse speed of the tool is increased. The reduced heat input facilitates the inhibition of

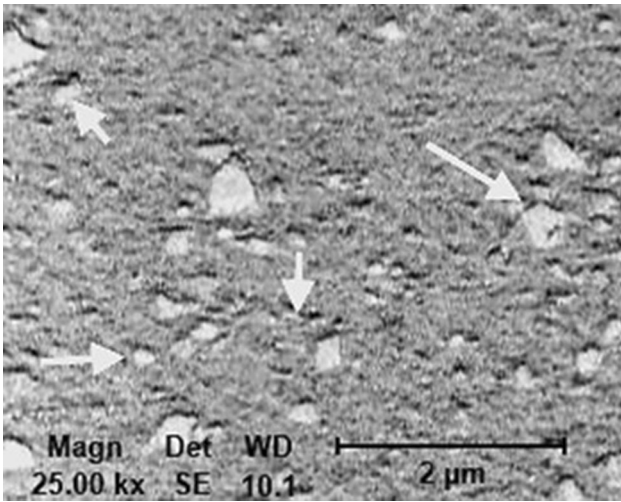


Fig. 9 Magnified SEM image showing the distribution of WC particles

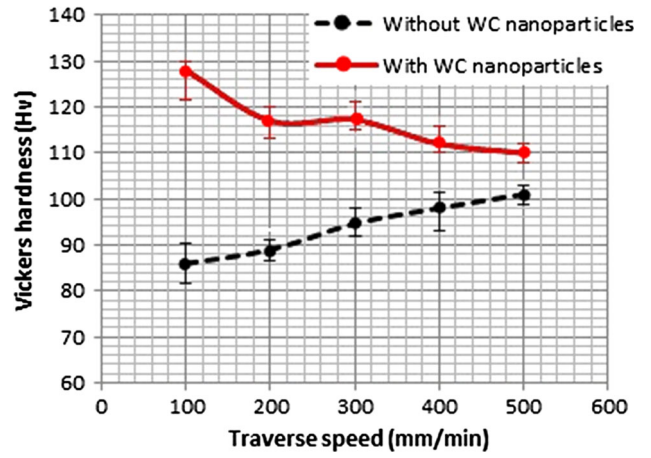


Fig. 12 Vickers microhardness profile for different traverse speeds with and without WC nanoparticles

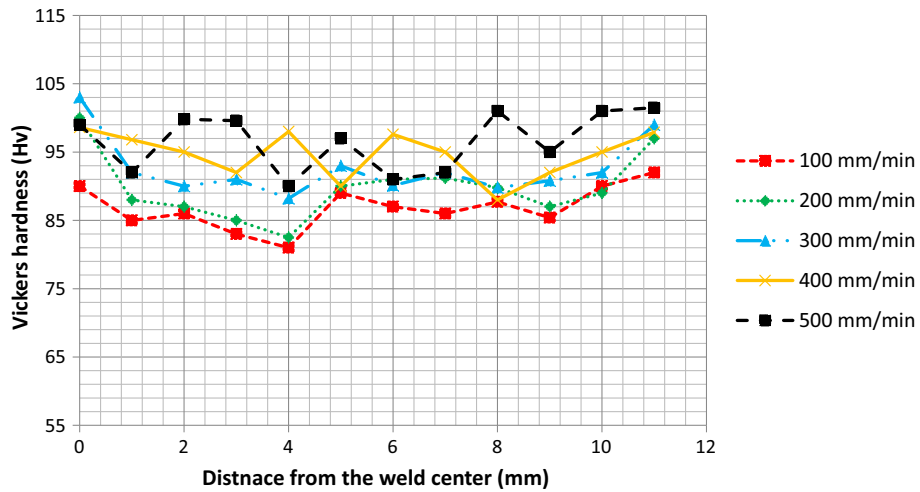


Fig. 10 The effect of tool traverses speed on the microhardness profile

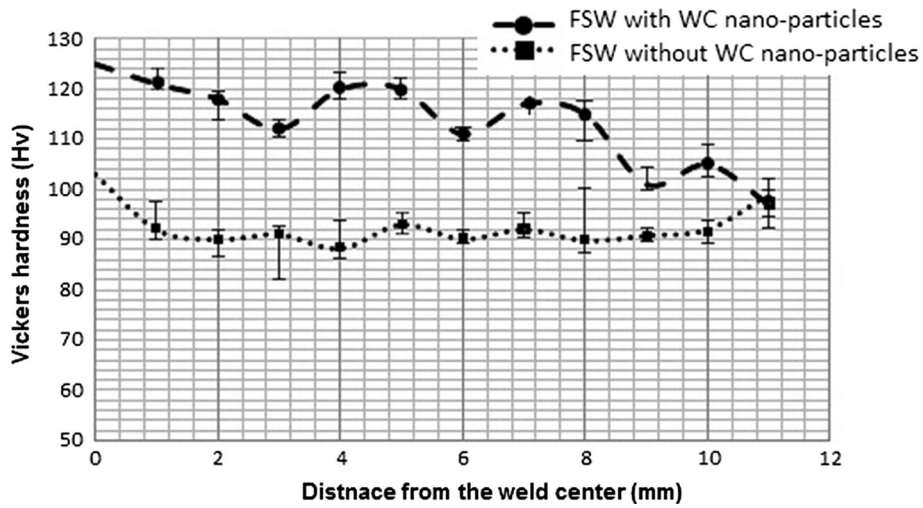


Fig. 11 The effect of the addition of WC nanoparticles at a constant traverse speed of 400 mm/min

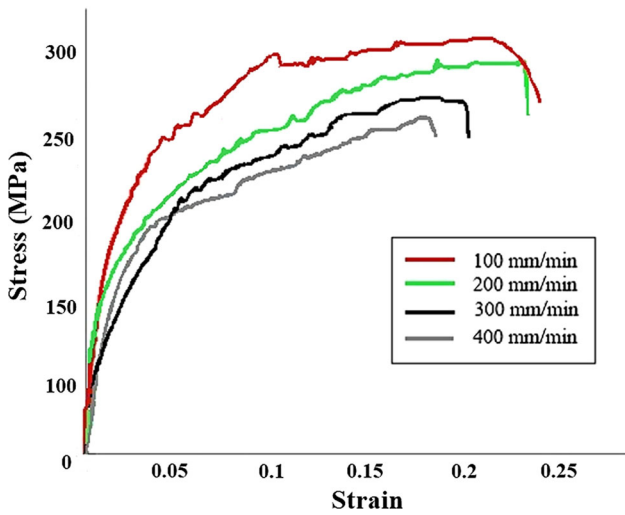


Fig. 13 Stress-strain plots showing the effect of traverse speed on the ultimate tensile strength of WC-reinforced welds

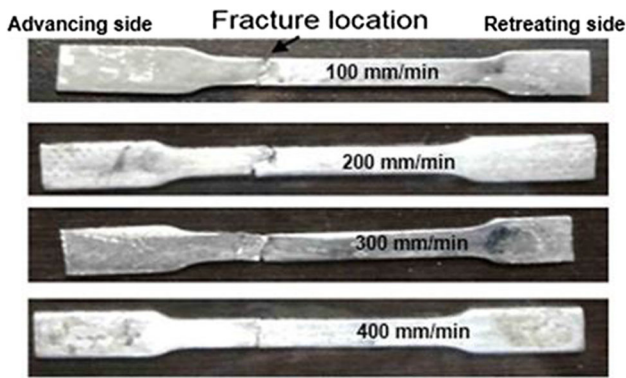


Fig. 14 Fracture location of WC-reinforced welds under axial loading as a function of tool traverse speed

grain growth and thereby improves the hardness of the welds. Meanwhile, the addition of WC nanoparticles to the SZ of AA5182 alloy essentially fixes the microhardness value of welds to a close approximate value as the traverse speed is increased. It can be adjudged that the WC reinforcements in the SZ of AA5182 alloy restrain the grains of the aluminum matrix to a definite size range as the heat input is reduced (as the traverse speed is increased); thus, giving rise to an approximately close hardness value.

3.3.2 Ultimate Tensile Strength and Fracture Assessment. Figure 13 shows the stress-strain curves of the reinforced welds as a function of the tool traverse speeds. Traverse speed has an inverse correlation with the ultimate tensile strength (UTS) of the reinforced welds. This occurrence can be attributed to the induced heat input and stirring actions attained in the welds. Sufficient heat input required for efficient material intermingling or stirring of the abutting materials and reinforcement is plausible at reduced/lower traverse speeds due to prolonged tool dwell period. This is adjudged to create better material flow, bonding and dispersion of reinforcement within the aluminum matrix; consequently, higher strength is obtained. Dislocation strengthening could as well be enhanced due to the likelihood of fragmented particle interaction with dislocations at reduced traverse speed. On the other hand, higher traverse speed may produce reduced heat input and cause inefficient intermingling of materials (abutting materials and reinforcement). This occurrence could have impaired the ultimate tensile strength of the reinforced welds at higher traverse speed. However, Moradi Faradonbeh et al. (Ref 20) this attributed to the better distribution of particulates that might be caused by low tool traverse speed.

Fracture locations of welds subjected to monotonic axial loading condition are shown in Fig. 14. Weld failures are observed to occur on the advancing side of the welds' stir zones. This occurrence could be attributed to the effect of traditionally minor plastic deformation at the advancing side of

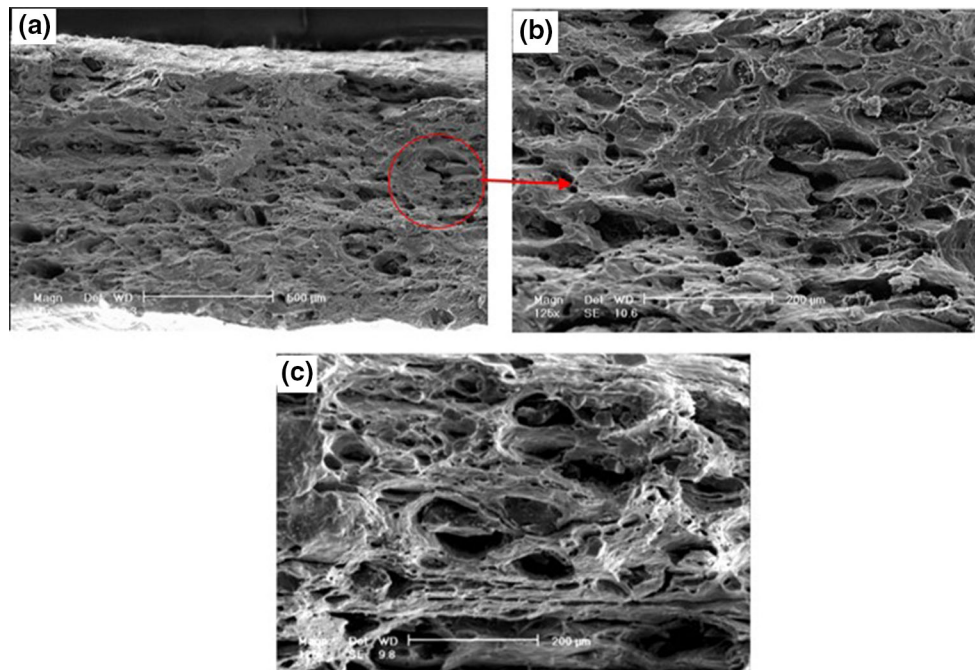


Fig. 15 SEM micrographs of failed weld surfaces at different tool traverse speeds, (a, b) 100 mm/min, (c) 400 mm/min

weld nuggets. This is in good agreement with the results expounded by Bodaghi et al. (Ref 9). However, in order to identify the fracture morphology of welds, the fracture surfaces of the welds are observed in a scanning electron microscope.

The fracture surfaces of the WC-reinforced joints (Fig. 15) show some dimples, few large voids and cleavage facet. This indicates that the welds fail by mixed ductile–brittle fracture modes. However, shallow dimples are present in Fig. 15(a) while substantial deep dimples are present Fig. 15(c). This occurrence may be attributed to the deformation of the stir zone and dispersion of WC reinforcement as the traverse speed is varied. High deformation and dispersion of WC ensue in welds obtained at a traverse speed of 100 mm/min. This absolutely causes better refinement of grains, high UTS and shallow dimples emerge on the fracture surfaces of such weld upon subjection to axial loading. Reinforced welds obtained at a traverse speed of 400 mm/min have weaker UTS and characteristic deep dimples with cleavage failure. Salemi Golezani et al. (Ref 21) investigated the effect of tool rotational speed on the fracture mode and found that the joints welded at lower rotational speeds show lower ductile fracture rather than the joints obtained at higher rotational speeds.

3.3.3 Wear Properties. The wear test was carried out to determine the variation of friction coefficient and wear rate on the reinforced welds. Table 1 shows the variation of wear rate as a function of the tool traverse speed for welds obtained with and without WC nanoparticles. It is revealed that the wear rate of the unreinforced weld ($9.207 \times 10^{-5} \text{ mm}^3/\text{Nm}$) is higher than that of the reinforced welds. A linear relationship exists between wear rate and traverse speed in the reinforced welds. This shows that grain refinement, even dispersion and fragmentation of WC nanoparticles enhance wear rate of AA5182 alloy as they are unique features of welds obtained at reduced

traverse speed. As revealed in section 3.2, the addition of WC nanoparticles to the alloy prevents grain growth in the resultant weld nugget, and this consequently leads to the enhancement of hardness which is responsible for the improvement of wear rate.

Some researchers (Ref 19, 22) reported that the presence of ceramic particles in the SZ of welds decreases the direct load between the specimen surface and the disk. Actually, load-bearing capacity of the hard reinforcing particles in the aluminum matrix decreases the direct load and subsequently decreases the wear rate of the reinforced welds. Furthermore, it is apparent that decreasing the tool traverse speed from 400 to 100 mm/min leads to a discernible difference in wear rate (from 5.293×10^{-5} to $1.95 \times 10^{-5} \text{ mm}^3/\text{Nm}$). This event can be attributed to the proper dispersion of WC nanoparticles in the weld due to a decrease in the tool traverse speed (Ref 19, 22, 23). Obviously, it is known that wear rate is a function of dispersion of particles and also grain size. As mentioned before, increasing the tool rotational speed and decreasing of traverse speed revealed a better dispersion of WC particles in the weld zone. This consequently improves the wear rate of the reinforced AA5182 alloy as favorable microstructure/grain refinement, homogeneous dispersion of WC nanoparticles and improved hardness properties are obtained.

Figure 16 shows the magnified worn weld surfaces (reinforced), while Fig. 17 depicts the close-up worn surfaces of welds obtained with and without WC nanoparticles as a function of the tool traverse speeds. The presence of WC particles during FSW led to the reduction of plastic deformation. It can be seen that welded specimens with WC nanoparticles exhibited high wear resistance more than the welds without WC nanoparticles. The worn surface of the base metal (Fig. 17a) exhibits a large amount of plastic deformation than the reinforced weld specimens. A decrease in the tool traverse speeds from 400 to 100 mm/min shows a corresponding decrease in the metal removal rate after wear test. This shows that better dispersion of reinforcement ensues at reduced traverse speed and reduced pit sizes are observed on the worn weld surface. It can be concluded that as the dispersion and fragmentation of WC nanoparticles increase, the size of pits on the worn weld surfaces decreases. These results confirmed the significant effect of WC nanoparticles distribution in AA5182 aluminum matrix on wear rate.

Figure 18 shows the graphs of friction coefficient as a function of slide distance for different traverse speeds. The comparison of the graphs in Fig. 18 shows that the friction coefficient of weld obtained with a traverse speed of 100 mm/min is lower than that of the other welds and the lowest

Table 1 Wear rate variation as a function of tool traverse speed with and without WC nanoparticles during FSW

Welded joint with	Traverse speed, mm/min	Wear rate, mm^3/Nm
...	100	9.207×10^{-5}
WC	400	5.293×10^{-5}
WC	300	3.875×10^{-5}
WC	100	1.95×10^{-5}

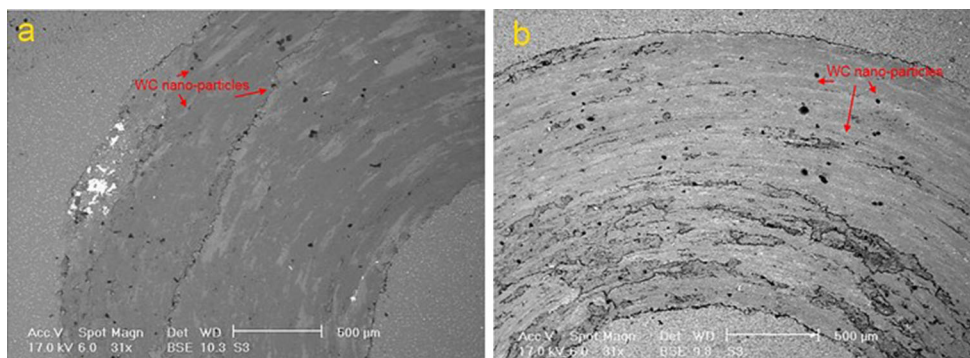


Fig. 16 Magnified worn surfaces of the reinforced joints

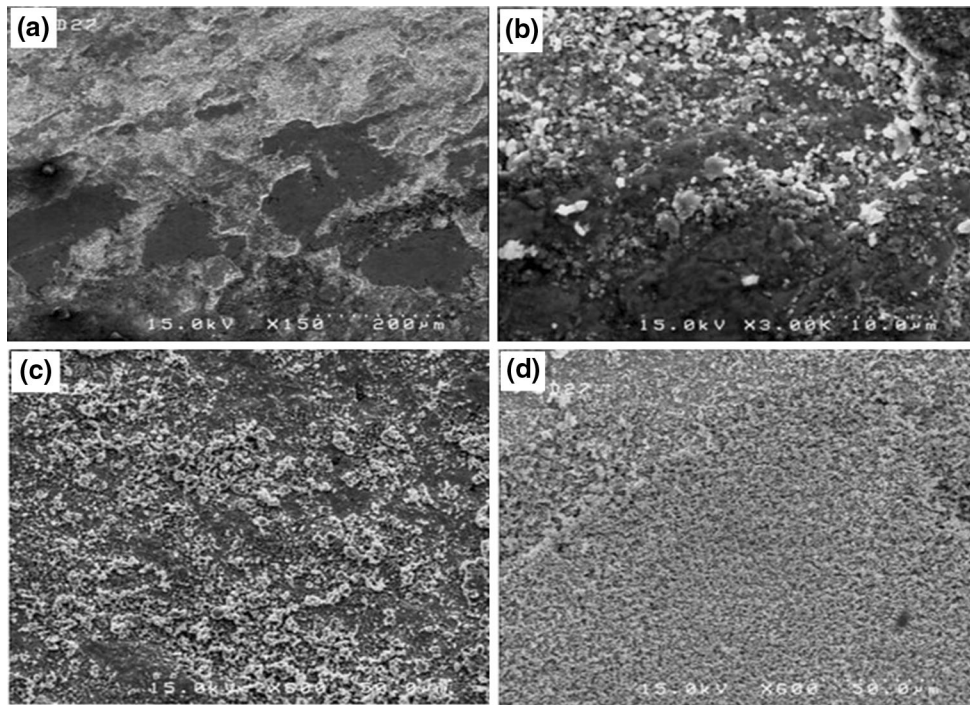


Fig. 17 SEM images of the worn surface of (a) base metal, (b) welded specimen at 400 mm/min traverse speed without WC nanoparticles, (c) welded at 400 mm/min traverse speed with WC nanoparticles and (d) welded at 100 mm/min traverse speed with WC nanoparticles

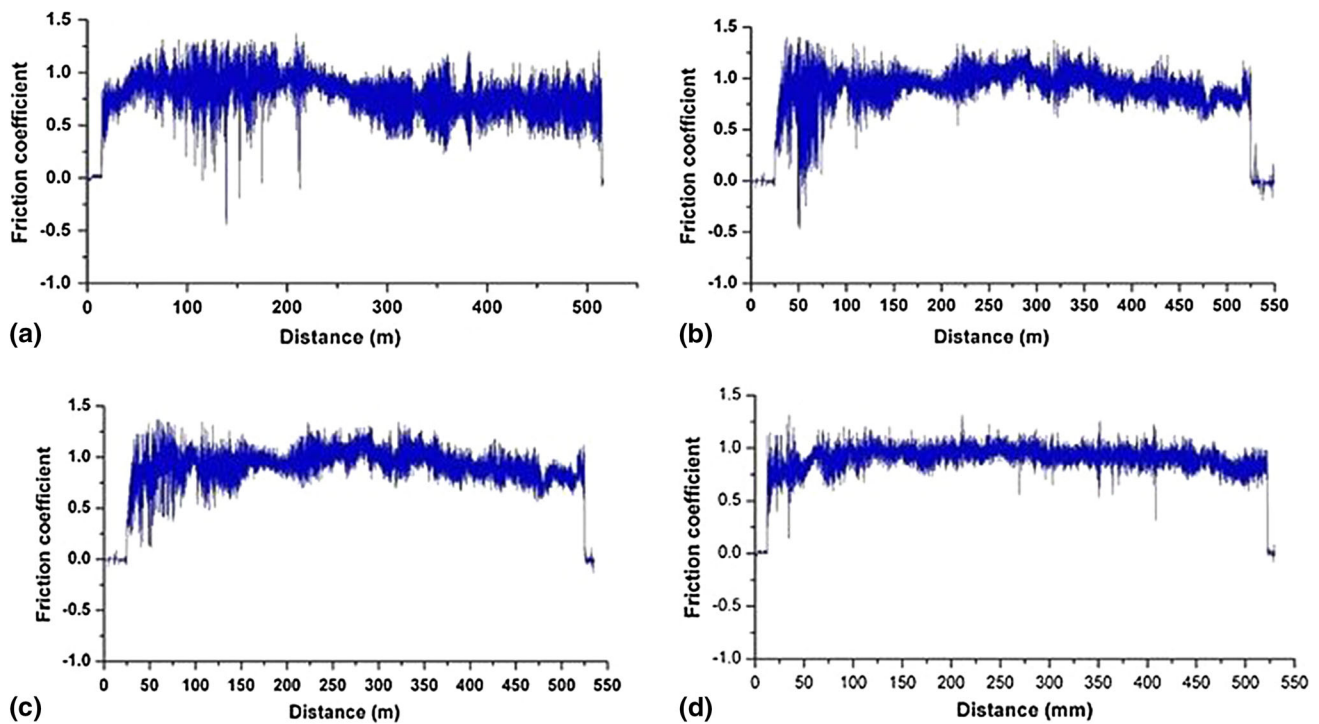


Fig. 18 Variation of friction coefficient as a function of distance at different traverse speeds, (a) 400, (b) 300, (c) 200 and (d) 100 mm/min

amplitude of friction coefficient profile is obtained with this weld. This result is most likely due to refined grain size/better fragmentation of reinforcement (see section 3.2) and homogeneous dispersion of WC nanoparticles at reduced tool traverse speed. However, a higher amplitude of friction profiles is observed at higher tool traverse speeds and this may likely be

as a result of the improper distribution of WC nanoparticles. The improper distribution of the WC nanoparticles will promote poor adhesion between the reinforcement and the aluminum matrix. Thus, during the wear testing process of such welds, the reinforcement agglomerated region in the weld will exhibit better/lower friction coefficient and reinforcement

depleted region will show higher friction coefficient and friction amplitude. Some researchers investigated the effect of reinforcement particle size on wear behavior. For instance Keneshloo et al. (Ref 24) found that the influence of nano-sized ceramic particulates on the weight loss during wear test was more than compared with that of the micron-sized particles.

4. Conclusions

The effects of traverse speed and WC nanoparticles on the mechanical, microstructural and tribological properties of friction stir welded AA5182 alloy were examined. The obtained results are summarized as follows:

- i. WC nanoparticles were successfully reinforced into the stir zone of friction stir welded AA5182 aluminum alloy without notable clustering and segregation of reinforcements.
- ii. The decrease in the level of tool traverse speed directly induces additional fragmentation of particles within the reinforced weld nugget of AA5182 alloy. The grains of the reinforced weld nugget were refined due to dynamic recrystallization created by the rotating tool and pinning influence of the WC nanoparticles.
- iii. WC nanoparticles significantly improve the hardness values of friction stir welded AA5182 alloy as compared to unreinforced welds. Likewise, an indirect relationship exists between tool traverse speed and ultimate tensile strength of WC-reinforced welds.
- iv. The addition of WC nanoparticles to the SZ of AA5182 alloy predominantly fixes the microhardness value of welds to a close approximate value as the traverse speed is increased beyond 200 mm/min. On the contrary, a direct correlation exists between hardness and tool traverse speed in welds obtained without reinforcements.
- v. Wear rate and wear coefficient are improved in AA5182 alloy reinforced with WC nanoparticles. Better dispersion of WC nanoparticles ensues at reduced traverse speed and this reduces pit sizes on the weld surface, while the weld's wear resistance is consequently improved.

References

1. O.S. Salih, H. Ou, W. Sun, and D.G. McCartney, A Review of Friction Stir Welding of Aluminum Matrix Composites, *Mater. Des.*, 2015, **86**, p 61–71
2. S.S. Mirjavadi, M. Alipour, S. Emamian, S. Kord, A.M.S. Hamouda, Praveennath G. Koppad, and R. Keshavamurthy, Influence of TiO₂ Nanoparticles Incorporation To Friction Stir Welded 5083 Aluminum Alloy on the Microstructure, Mechanical Properties and Wear Resistance, *J. Alloy. Compd.*, 2017, **712**, p 795–803
3. N. Yuvaraj, S. Aravindan, and Vipin, Fabrication of Al5083/B₄C Surface Composite by Friction Stir Processing and Its Tribological Characterization, *J. Mater. Res. Technol.*, 2015, **4**(4), p 398–410
4. I. Sudhakar, V. Madhu, G. Madhusudhan Reddy, and K. Srinivasa Rao, Enhancement of Wear and Ballistic Resistance of Armour Grade AA7075 Aluminum Alloy Using Friction Stir Processing, *Def. Technol.*, 2015, **11**, p 10–17
5. R. Palanivel, I. Dinaharan, R.F. Laubscher, and J. Paulo Davim, Influence of Boron Nitride Nanoparticles on Microstructure and Wear Behavior of AA6082/TiB₂ Hybrid Aluminum Composites Synthesized by Friction Stir Processing, *Mater. Des.*, 2016, **106**, p 195–204

6. S. Sahraeinejad, H. Izadi, M. Haghshenas, and A.P. Gerlich, Fabrication of Metal Matrix Composites by Friction Stir Processing with Different Particles and Processing Parameters, *Mater. Sci. Eng., A*, 2014, **626**, p 505–513
7. S. Selvakumar, I. Dinaharan, R. Palanivel, and B.G. Babu, Characterization of Molybdenum Particles Reinforced Al6082 Aluminum Matrix Composites with Improved Ductility Produced Using Friction Stir Processing, *Mater. Charact.*, 2017, **125**, p 13–22
8. S. Selvakumar, I. Dinaharan, R. Palanivel, and B. Ganesh Babu, Development of Stainless Steel Particulate Reinforced AA6082 Aluminium Matrix Composites with Enhanced Ductility Using Friction Stir Processing, *Mater. Sci. Eng., A*, 2017, **685**, p 317–326
9. M. Bodaghi and K. Dehghani, Friction Stir Welding of AA5052: The Effects of SiC Nano-Particles Addition, *Int. J. Adv. Manuf. Technol.*, 2016, **88**(9–12), p 2651–2660
10. M. Sarkari Khorrami, M. Kazeminezhad, and A.H. Kokabi, Thermal Stability of Aluminum After Friction Stir Processing with SiC Nanoparticles, *Mater. Des.*, 2015, **80**, p 41–50
11. M. Paidar and M. Laali Sarab, Friction Stir Spot Welding of 2024-T3 Aluminum Alloy with SiC Nanoparticles, *J. Mech. Sci. Technol.*, 2016, **30**(1), p 365–370
12. M. Mohammadi-pour, A. Khodabandeh, S. Mohammadi-pour, and M. Paidar, Microstructure and Mechanical Properties of Joints Welded by Friction-Stir Welding in Aluminum Alloy 7075-T6 Plates for Aerospace Application, *Rare Met.*, 2016, <https://doi.org/10.1007/s12598-016-0692-9>
13. M. Paidar, A. Khodabandeh, H. Najafi, and A. Sabour Rouh-aghdam, An Investigation on Mechanical and Metallurgical Properties of 2024-T3 Aluminum Alloy Spot Friction Welds, *Int. J. Adv. Manuf. Technol.*, 2015, **80**(80), p 183–196
14. A. Salemi Golezani, R. Vatankhah Barenji, A. Heidarzadeh, and H. Pouraliakbar, Elucidating of Tool Rotational Speed in Friction Stir Welding of 7020-T6 Aluminum Alloy, *Int. J. Adv. Manuf. Technol.*, 2015, **81**, p 1155–1164
15. R. Akbari, S. Mirdamadi, A. Khodabandeh, and M. Paidar, A Study on Mechanical and Microstructural Properties of Dissimilar FSWed Joints of AA5251–AA5083 Plates, *Int. J. Mater. Res.*, 2016, **107**, p 752–761
16. J.A. Al-Jarrah, S. Swalha, T.A. Mansour, M. Ibrahim, M. Al-Rashdan, and D.A. Al-Qahsi, Welding Equality and Mechanical Properties of Aluminum Alloys Joints Prepared by Friction Stir Welding, *Mater. Des.*, 2014, **56**, p 929–936
17. J.J. Moses, I. Dinaharan, and S.J. Sekhar, Production and Characterization of Titanium Carbide Particulate Reinforced AA6061 Aluminum Alloy Composites Using Stir Casting, *Kovove Mater.*, 2016, **54**, p 257–267
18. A. Heidarzadeha, H. Pouraliakbar, S. Mahdavic, and M.R. Jandaghi, Ceramic Nanoparticles Addition in Pure Copper Plate: FSP Approach, Microstructure Evolution and Texture Study Using EBSD, *Ceram. Int.*, 2018, **44**, p 3128–3133
19. H. Eftekharinia, A.A. Amadeh, A. Khodabandeh, and M. Paidar, Microstructure and Wear Behavior of AA6061/SiC Surface Composite Fabricated Via Friction Stir Processing with Different Pins and Passes, *Rare Met.*, 2016, <https://doi.org/10.1007/s12598-016-0691-x>
20. A. Moradi Faradonbeh, M. Shamanian, H. Edris, M. Paidar, and Y. Bozkurt, Friction Stir Welding of Al-B₄C Composite Fabricated by Accumulative Roll Bonding: Evaluation of Microstructure and Mechanical Behavior, *J. Mater. Eng. Perform.*, 2018, **27**(2), p 835–846
21. A. Salemi Golezani, R. Vatankhah Barenji, A. Heidarzadeh, and H. Pouraliakbar, Elucidating of Tool Rotational Speed in Friction Stir Welding of 7020-T6 Aluminum Alloy, *Int. J. Adv. Manuf. Technol.*, 2015, **81**, p 1155–1164
22. M. Farahmand Nikoo, H. Azizi, N. Parvin, and H. Yousefpour Naghibi, The Influence of Heat Treatment on Microstructure and Wear Properties of Friction Stir Welded AA6061-T6/Al₂O₃ Nanocomposite Joint at Four Different Traversing Speed, *J. Manuf. Process.*, 2016, **22**, p 90–98
23. M. Navazani and K. Dehghani, Fabrication of Mg-ZrO₂ Surface Layer Composites by Friction Stir Processing, *J. Mater. Process. Technol.*, 2016, **229**, p 439–449
24. M. Keneshloo, M. Paidar, and M. Taheri, Role of SiC Ceramic Particles on the Physical and Mechanical Properties of Al-4%Cu Metal Matrix Composite Fabricated Via Mechanical Alloying, *J. Compos. Mater.*, 2017, **51**(9), p 1285–1298